Journal of Zhejiang University-SCIENCE B (Biomedicine & Biotechnology) *2024 25(5):410-421*
www.jzus.zju.edu.cn; www.springer.com/journal/11585
E-mail: jzus_b@zju.edu.cn

Research Article

https://doi.org/10.1631/jzus.B2300579

Check for updates

Adrenal pheochromocytoma impacts three main pathways: cysteine-methionine, pyrimidine, and tyrosine metabolism

Chong LAI[1*], Qingling YANG[2*], Yunuo ZHANG[2], Renjie GONG[3], Majie WANG[4], Jiankang LI[5], Maode LAI[6], Qingrong SUN[6✉]

[1]*Department of Urology, the First Affiliated Hospital, Zhejiang University School of Medicine, Hangzhou 310003, China*
[2]*School of Basic Medical Sciences and Clinical Pharmacy, China Pharmaceutical University, Nanjing 210009, China*
[3]*Department of Laboratory Medicine, the First Affiliated Hospital, Zhejiang University School of Medicine, Hangzhou 310003, China*
[4]*Laboratory of Behavioral Neuroscience, Ningbo Kangning Hospital, Ningbo Institute of Microcirculation and Henbane, School of Medicine, Ningbo University, Ningbo 315201, China*
[5]*Xi'an Key Laboratory of Stem Cell and Regenerative Medicine, Institute of Medical Research, Northwestern Polytechnical University, Xi'an 710072, China*
[6]*Department of Pathology, Research Unit of Intelligence Classification of Tumor Pathology and Precision Therapy, Chinese Academy of Medical Sciences Key Laboratory of Disease Proteomics of Zhejiang Province, Zhejiang University School of Medicine, Hangzhou 310058, China*

Abstract: Pheochromocytomas and paragangliomas (PPGLs) cause symptoms by altering the circulation levels of catecholamines and peptide hormones. Currently, the diagnosis of PPGLs relies on diagnostic imaging and the detection of catecholamines. In this study, we used ultra-performance liquid chromatography (UPLC)/quadrupole time-of-flight mass spectrometry (Q-TOF MS) analysis to identify and measure the perioperative differential metabolites in the plasma of adrenal pheochromocytoma patients. We identified differentially expressed genes by comparing the transcriptomic data of pheochromocytoma with the normal adrenal medulla. Through conducting two steps of metabolomics analysis, we identified 111 differential metabolites between the healthy group and the patient group, among which 53 metabolites were validated. By integrating the information of differential metabolites and differentially expressed genes, we inferred that the cysteine-methionine, pyrimidine, and tyrosine metabolism pathways were the three main metabolic pathways altered by the neoplasm. The analysis of transcription levels revealed that the tyrosine and cysteine-methionine metabolism pathways were downregulated in pheochromocytoma, whereas the pyrimidine pathway showed no significant difference. Finally, we developed an optimized diagnostic model of two metabolites, L-dihydroorotic acid and vanylglycol. Our results for these metabolites suggest that they may serve as potential clinical biomarkers and can be used to supplement and improve the diagnosis of pheochromocytoma.

Key words: Pheochromocytoma and paraganglioma (PPGL); Metabolomics; Gene set variation analysis; L-Dihydroorotic acid; Vanylglycol

1 Introduction

Pheochromocytomas (PCCs) and paragangliomas (PPGLs) are neoplasms composed of chromaffin cells in the adrenal medulla (Fig. 1) or from extra-adrenal sympathetic and parasympathetic paraganglia, which synthesize and release catecholamines and occasionally peptide hormones. The incidence of PPGL ranges between 2 and 8 per million, with a prevalence between 1:2500 and 1:6500 (Aygun and Uludag, 2020). Secondary hypertension caused by paroxysmal vasoconstriction occurs in approximately two-thirds of PPGL patients (Baxter et al., 1992; Wu HY et al., 2021) and even presents as a recurrent symptom in PCC patients with abdominal aortic aneurysm (Zhao et al., 2021). Excess catecholamine results in a broad spectrum of clinical symptoms that depend on the overall catecholamine surplus and its duration. The typical manifestation is the triad of paroxysmal headache, sweating, and palpitations. Hormone-dependent cardiovascular complications as well as metabolic alterations are the

✉ Qingrong SUN, sunqingrong@zju.edu.cn
* The two authors contributed equally to this work
Chong LAI, https://orcid.org/0000-0002-6581-9987
Qingrong SUN, https://orcid.org/0000-0002-1616-7978

Received Aug. 14, 2023; Revision accepted Oct. 8, 2023;
Crosschecked Jan. 15, 2024; Published online Mar. 12, 2024

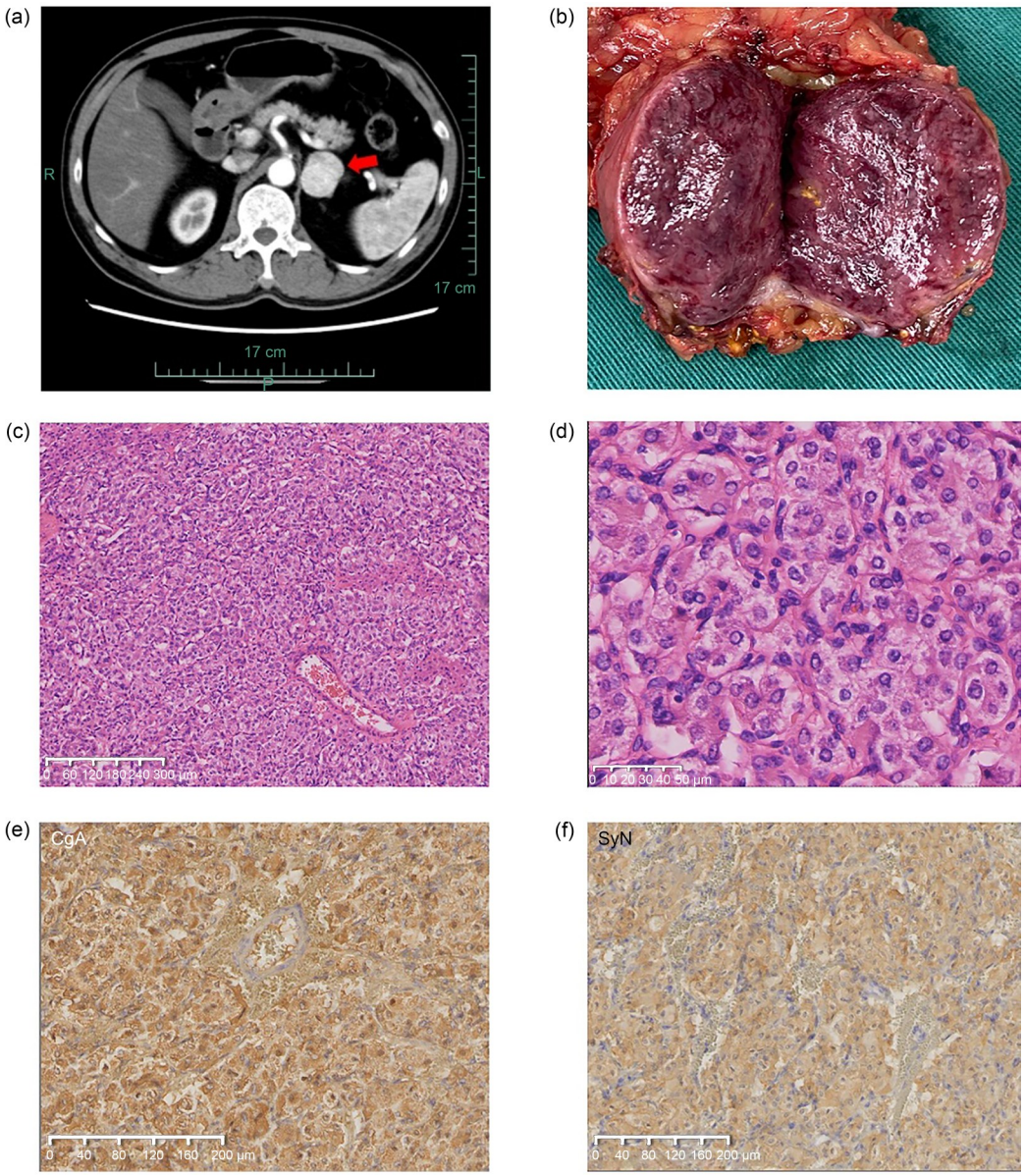

Fig. 1 Pheochromacytoma from the adrenal medulla of a 59-year-old male patient. (a) Axial arterial phase computed tomography (CT) image (the red arrow indicates the tumor, which is an oval mass (3.5 cm×3.0 cm) in the left adrenal gland near the aorta). P: posterior; R: right; L: left. (b) Pheochromacytoma gross. (c) Haematoxylin and eosin (H&E) image at low magnification. (d) H&E image at high magnification. (e) Immunohistochemical staining with chromogranin A (CgA) antibody. (f) Immunohistochemical staining with synaptophysin (SyN) antibody.

main drivers of PPGL-associated morbidity and mortality (Zuber et al., 2011). Elevated glucose and diabetes were also found in long-lasting PPGLs (Farrugia and Charalampopoulos, 2019). The diagnostic work-up of PPGLs includes detection of plasma or urinary metanephrines with or without catecholamines and chromogranin A, followed by imaging studies (B ultrasound, computed tomography (CT), and magnetic resonance imaging (MRI)). With the widespread utilization of general health examination and the development of medical imaging techniques, smaller asymptomatic PCC cases are increasingly discovered. Although surgery currently represents the only modality of ultimate cure, pharmacologic preoperative treatment targeted at vessels and the heart remains the mainstay of successful outcomes. To control hypertension levels and/or tachyarrhythmia prior to operation, even in preoperative normotensive cases, it is recommended that patients take

oral α-blockade for 10–14 d until the blood pressure (BP) and other symptoms have stabilized (Zuber et al., 2011; Naranjo et al., 2017).

For PPGL patients, the alteration of specific small molecules within the biological system (metabolomics) is crucial to pathophysiology and has the potential to become a routine addition to histology and genomics for precise diagnostic evaluation (Eisenhofer et al., 2004). The perioperative variation trend of metabolomics may reveal the underlying cellular dysfunction, recovery, and long-term impact of this neoplasm on patients. With the evolution of biochemical detection, especially the introduction of liquid chromatography-tandem mass spectrometry (LC-MS/MS), metabolomics alterations in PPGLs have been widely studied. Dwight et al. (2019) reviewed metabolic studies before 2019 and highlighted the value of metabolomics as an important target for identifying the metabolic defects of PPGLs. However, most of these studies had focused on Krebs cycle enzymes, mitochondrial regulators, and oncogenic metabolites (Jochmanova and Pacak, 2016; Remacha et al., 2017), while few works had reported detailed metabolic changes or explored characteristic patterns in the metabolic pathways. In the current study, we first integrated the metabolomics data of patient plasma with differentially expressed gene (DEG) screening of PCC tissues to find the main alterations of metabolic pathways. Preoperative differential metabolites were compared with those of postoperative patients to highlight PCC-associated metabolites.

2 Materials and methods

2.1 Study design and procedures

The patients in this study with adrenal tumors were diagnosed and operated at the Department of Urology, the First Affiliated Hospital, Zhejiang University School of Medicine, Hangzhou, China, between 2017 and 2019. Controls matched for gender and age of healthy people, who were taking routine annual examination and were cleared for any disease, were also recruited at the sampling stage.

In the discovery set, 293 plasma samples were collected, including 146 healthy people and 147 preoperative patients with adrenal tumors (100 adrenal cortical adenoma, 9 PCC, 15 myelolipoma and ganglioneuroma, 2 adrenocortical carcinoma, and 5 metastatic tumors, and 16 other tumors). The validation set included 319 participants from the same center, including 154 healthy people and 165 preoperative patients with adrenal tumors (121 adrenal cortical adenomas, 22 PCC, and 22 myelolipoma and ganglioneuroma). In this study, we only analyzed metabolic changes in PCC patients. In 31 cases of PCC, 12 were males and 19 were females. Among the 12 male cases with an average age of 43.75 years, 8 had a tumor on the left adrenal gland and 4 on the right. From the imaging records, among the 19 female patients with an average age of 50.78 years, 9 had a tumor on the left adrenal gland and 10 on the right. In this study, all of these 19 patients had hypertension (based on guidelines from the Chinese Society of Cardiology). Eleven cases had typical paroxysmal symptoms (such as paroxysmal dizziness, syncope, palpitation, and sweating), accounting for 35.5% of all PCC patients. One-third of PCC patients presented no symptoms except hypertension in some patients. Diagnosis was clarified in all cases through CT or MRI, while 18 cases were subject to accidental diagnosis upon admission to hospital for other medical conditions irrelevant to PCC or routine checkup. The largest diameter of all tumors was 2.0–10.5 cm and the average diameter was 5.0 cm.

2.2 Experimental design

In this study, plasma samples were drawn in the morning after overnight fasting for at least 8 h and collected into sodium citrate solution tubes. All plasma samples were sub-packaged in 1.5-mL Eppendorf (EP) tubes and then stored at −80 ℃. The samples were thawed slowly in a refrigerator at 4 ℃ for 30 min for analysis. Then, 50 μL plasma from every sample and 150 μL methanol were mixed with 100 ng/mL L-2-chlorophenylalanine and 1 μg/mL ketoprofen and vortexed for 30 s, followed by placing them into a cryogenic high-speed centrifuge (13 000 r/min for 10 min at 4 ℃). Subsequently, we equally divided 150 μL aliquot of the supernatant into another two 1.5-mL tubes, and dried them under a gentle stream of nitrogen at room temperature, which redissolved in 70 μL methanol solution. Finally, we vortexed two tubes of solution for 30 s and placed them into a cryogenic high-speed centrifuge (13 000 r/min for 10 min at 4 ℃). A total of 50 μL of the supernatant was transferred into the vials. The 1 μL aliquot of the supernatant fraction was injected into the ultra-performance liquid

chromatography (UPLC)/quadrupole time-of-flight mass spectrometry (Q-TOF MS) for untargeted analysis. In addition, 10 μL of each sample was taken and mixed as quality control samples. All details were shown in Fig. 2.

2.3 UPLC/Q-TOF MS analysis

UPLC/Q-TOF MS analysis was performed on an Agilent 1290 liquid chromatographic instrument (Agilent Technologies, USA) coupled to an Agilent 6545 Q-TOF MS system (Agilent Technologies) in both the positive and negative ionization modes. The column employed was Waters BEH C8 (100 mm×2.1 mm, 1.7 μm; Waters Corporation, Milford, MA, USA) and the temperature was maintained at 50 °C. The mobile phases used were 0.1% (volume fraction) formic acid in acetonitrile (A) and 0.1% formic acid in water (B) for the positive ion mode, and 5 mmol/L ammonium acetate in acetonitrile (A) and 5 mmol/L ammonium acetate in water (B) for the negative ion mode. The gradient program was optimized as follows: 0–1 min, 5% A; 1–4 min, 5%–30% A; 4–9 min, 30%–90% A; 9–10 min, 90%–100% A; 10–12 min, 100% A. The running time was 12 min, and the retention time was 3 min. The flow rate was 0.4 mL/min, the autosampler was maintained at 7 °C, and the injection volume was 1 μL.

For MS analysis, the following conditions were set: collision voltage, 120 V; drying gas flow rate, 12 L/min; temperature, 350 °C; nebulizer gas, 241.255 kPa gauge. The sheath gas temperature was 375 °C, and the sheath

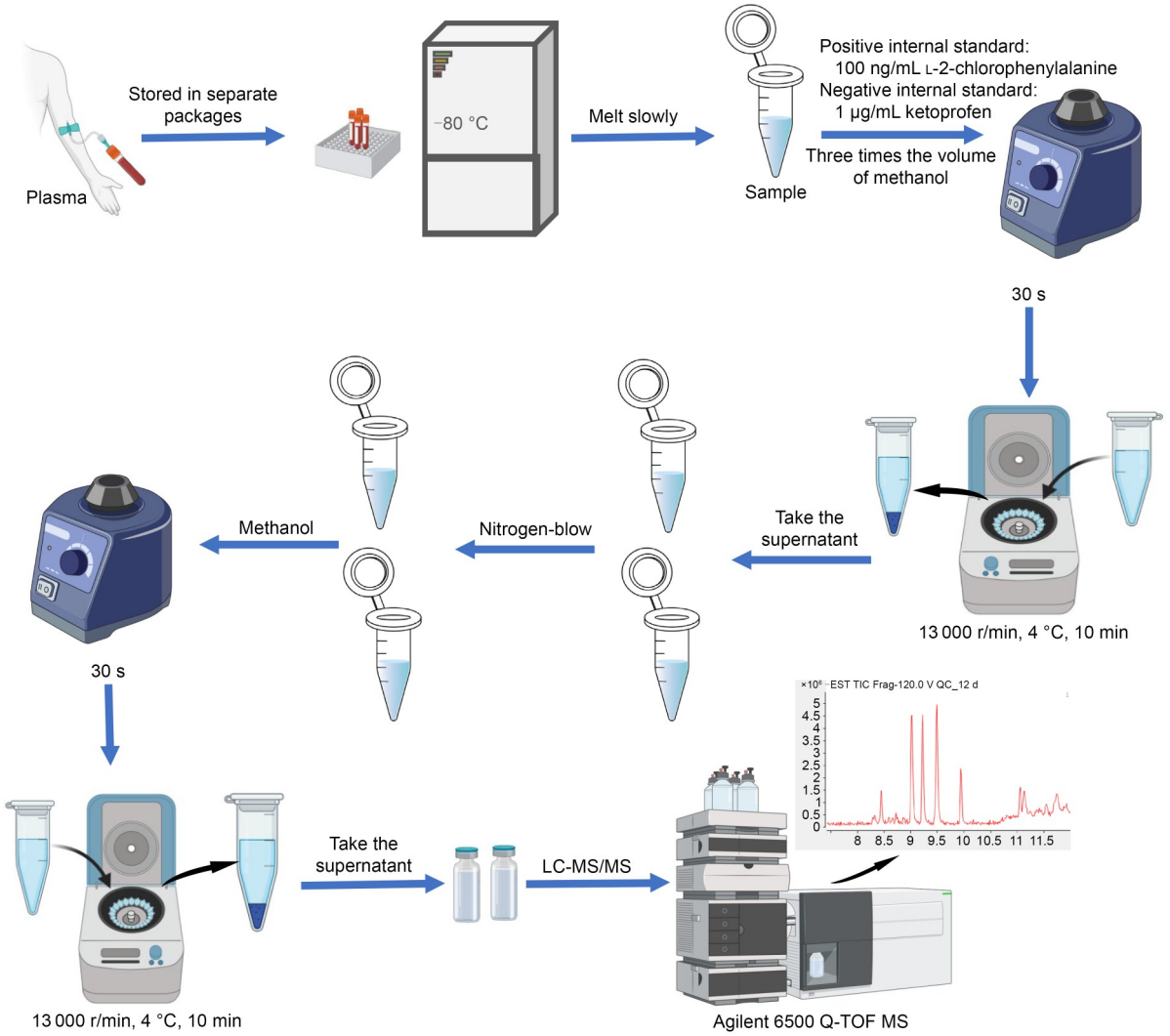

Fig. 2 Schematic of the overall experimental procedure. Flowchart from sample treatment to analysis. LC-MS/MS: liquid chromatography-tandem mass spectrometry; Q-TOF MS: quadrupole/time-of-flight mass spectrometry.

gas flow rate was 12 L/min. The capillary voltage was set at 3500 V and the nozzle voltage was 1500 V. MS data were collected 1.5 times per second in full scan mode, and the range of the scan was from mass-to-charge ratio (m/z) 100 to 1000. The reference ions in the positive ion mode were m/z 121.0508 and m/z 922.0098, and the reference ions in the negative ion mode were m/z 112.9855 and m/z 980.0163.

2.4 Untargeted metabolomics analysis

All data were acquired employing Agilent 6545 MassHunter Workstation Software. Then, the acquired data were exported to mzdata format and preprocessed through R-4.2.1 by the XCMS package. We used supervised orthogonal partial least squares-discriminant analysis (OPLS-DA) and Wilcoxon Signed Rank Test to identify differential metabolites by the threshold variable importance in the projection (VIP)>1 and adjusted P-value<0.05 (false discovery rate (FDR), corrected by Benjamini and Hochberg (1995)). We annotated the primary and secondary profiles of the differential metabolite peaks based on the Human Metabolome Database (https://hmdb.ca) and Agilent PCDL Manager B.07.00 database.

For the metabolic pathway analysis, we located the differential metabolites in pathways by the Kyoto Encyclopedia of Genes and Genomes (KEGG) database, and the gene–disease relationship networks of differential metabolites were analyzed by MetaboAnalyst 5.0 (https://www.metaboanalyst.ca).

For the screened differential metabolites, we evaluated the diagnosis contribution of the three metabolites between PCC and healthy samples based on the Least Absolute Shrinkage and Selection Operator (LASSO) model. The area under curve (AUC) values of multiple metabolite combinations and single metabolites for the diagnosis of PCC were shown in the receiver operating characteristic (ROC) curve.

2.5 Differentially expressed gene analysis

We downloaded the PCC messenger RNA (mRNA) expression dataset from the Gene Expression Omnibus (GEO) database. We identified DEGs between PCC and healthy samples from dataset GSE19422 (López-Jiménez et al., 2010) using Student's t-test. The threshold of FDR<0.05 and mean gene-expression fold change>1.2 was used to identify the DEGs.

2.6 Pathway enrichment analysis

Firstly, we used the clusterProfiler (Wu TZ et al., 2021) tool of R language to perform enrichment analysis and visualization for DEGs based on KEGG and the Gene Ontology (GO) databases. The function enrichGO of clusterProfiler was used for enrichment analysis and set FDR<0.05 The function barplot in clusterProfiler was implemented to visualize the enrichment results and set the top 20 significant pathways. Then, we downloaded "c2.cp.kegg.v7.1.symbols.gmt" and "h.all.v7.4.entrez.gmt.txt" from the MSigDB database (https://www.gsea-msigdb.org/gsea/index.jsp) and selected the metabolic pathway gene sets. Based on these gene sets and mRNA expression data, we used the gene set variation analysis (GSVA) algorithm (Hänzelmann et al., 2013) to score every sample in each metabolic pathway. Finally, we used the Wilcoxon Signed Rank Test to identify differential metabolic pathways by GSVA score with a P-value of <0.05.

3 Results

3.1 Identification of potential metabolic biomarkers

From the UPLC/Q-TOF MS data, we found 2480 and 2582 signal ions of the discovery set and the validation set, respectively. According to differential analysis, in the discovery set, a total of 322 differential ions were screened in the healthy and PCC preoperative plasma samples, and a total of 253 differential ions were screened in the preoperative and postoperative PCC plasma samples. In the validation set, a total of 510 differential ions were screened in the healthy and PCC preoperative plasma samples, and 453 differential ions were screened in the preoperative and postoperative PCC plasma samples. After obtaining the secondary mass spectra, the differential ions were compared to the Human Metabolome Database and Agilent PCDL Manager B.07.00 data. We identified 53 differential metabolites between healthy and PCC preoperative samples in the discovery set and the validation set (Fig. 3a). A total of 53 differential metabolites were found between the preoperative and the postoperative PCC plasma samples (Fig. 3b). We found that a total of 103 differential metabolites appeared stably in both the discovery set and the validation set, of which 53 differential metabolites were present in the healthy

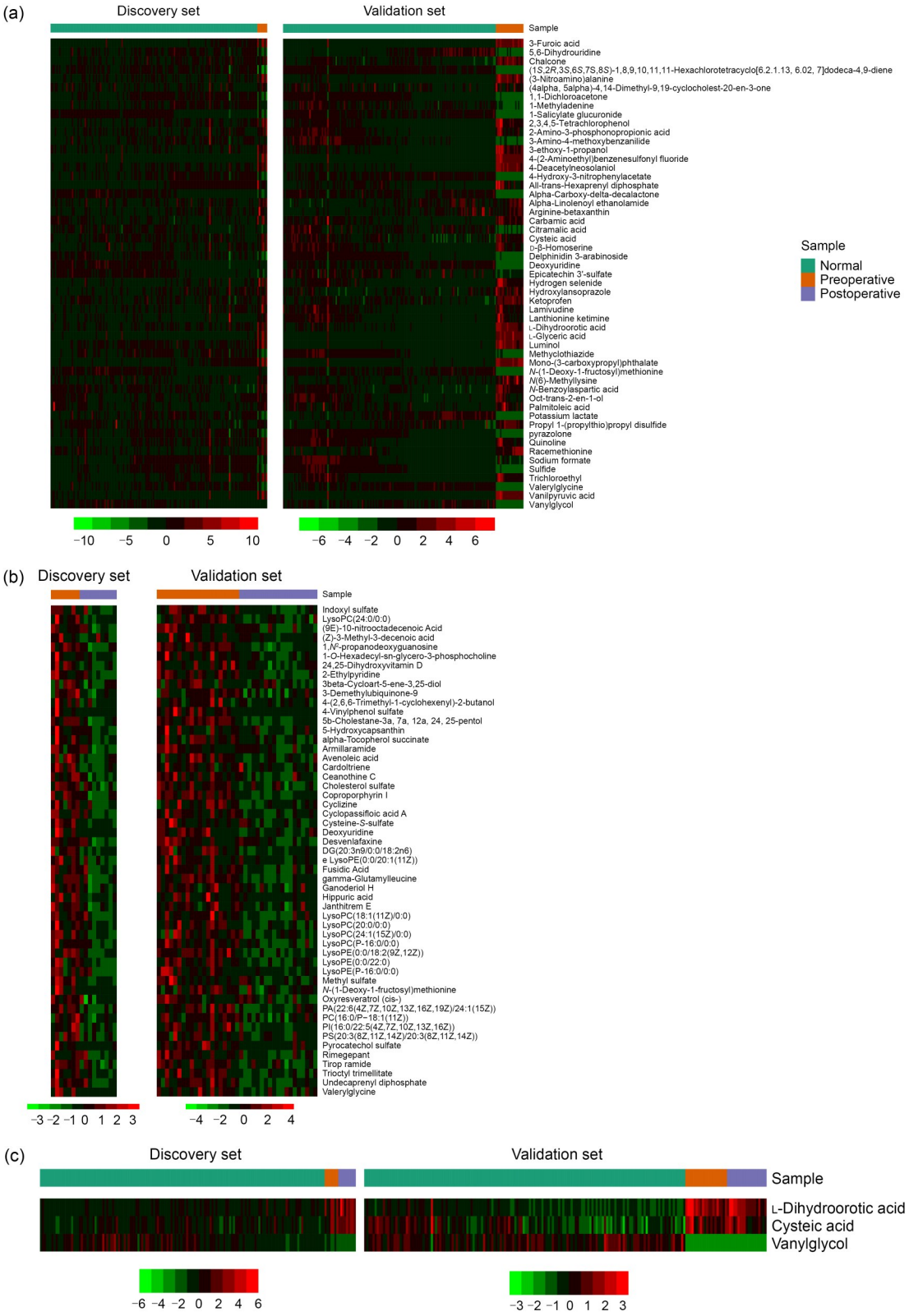

Fig. 3 Different metabolites in the discovery set and the validation set. (a) Differential metabolites between the healthy and pheochromocytoma (PCC) preoperative groups. (b) Differential metabolites between the PCC preoperative and PCC postoperative groups. (c) Three different metabolites in the metabolic pathways.

and PCC preoperative groups, 53 differential metabolites were present in the PCC preoperative and postoperative groups, and 3 differential metabolites were present in discovery set and validation set (Fig. 3c). These 103 differential metabolites could be considered as potential biomarkers. From Fig. 3b, we found that differential metabolites were significantly downregulated in the postoperative group compared with those in the preoperative group. The differential analysis results are all presented in Tables S1–S6.

3.2 Differentially expressed gene analysis

In the GSE19422 dataset, 61 PCC and 6 heathy samples were selected for differential analysis. We identified 3830 DEGs (1814 upregulated and 2016 downregulated in PCC) between the two groups (Table S7). Among them, 42 genes could match the corresponding GO enrichment, and the upregulated genes were mainly involved in the metabolic pathways related to neural activities involving axons, synapses, and neurotransmitters, which might have a correlation with the origin of PCC (Lee et al., 2005; Huang et al., 2022; Chen and Wang, 2023). The downregulated genes are related to various metabolisms, including those of cholesterol, fatty acid, ethanol, sterol hormones, and nucleotides. The genetic alteration also conformed to the metabolic changes of PCC patients (Jochmanova and Pacak, 2016; Erlic and Beuschlein, 2019) (Fig. S1).

3.3 Metabolic pathway analysis

A pathway analysis was performed for 53 differential metabolites that were stabilized in the healthy and PCC preoperative groups. We found that three metabolites were successfully matched to relevant metabolic disorder pathways, namely, L-dihydroorotic acid, cysteic acid, and vanylglycol (Fig. 3c). The pathway enrichment results showed that the major altered pathways were the cysteine-methionine metabolism pathway, tyrosine metabolism pathway, and pyrimidine metabolism pathway (Fig. 4a). As shown in Fig. 4b, 41 DEGs were matched to metabolic pathways and 29 of them were downregulated in PCC. The above results were also validated in Figs. 4c and 4d.

3.4 Diagnostic model construction

Through the LASSO model developed based on the above three metabolites, we found that the contribution coefficient of cysteic acid in both the discovery set and the validation set was 0 (Fig. 5a). We evaluated this model based on ROC curve and found that its AUC values in the discovery set and validation set were 0.888 and 0.998, respectively (Figs. 5b and 5c). We then redesigned the LASSO regression model based on merely L-dihydroorotic acid and vanylglycol, and found that the AUC values in the discovery set and validation set were 0.893 and 1.000, respectively (Figs. 5d and 5e). To verify the diagnostic ability of a single metabolite, ROC curves were drawn for a single metabolite based on the Youden index (Fluss et al., 2005). The AUC values of L-dihydroorotic acid and vanylglycol were greater than 0.8 in both the discovery set and the validation set (Fig. S2). The numbers were eligible for the effective indication of PCC. Therefore, the combined application of the two substances could obtain better sensitivity and specificity in the prediction for PCC.

4 Discussion

PCCs are catecholamine-producing tumors with complicated metabolism. Excessive circulating levels of catecholamines and their metabolites can lead to organ-specific hypertensive complications of hypercatecholaminemia, with devastating effects on multiple body systems, including but not limited to cardiovascular, cerebrovascular, renal, and ocular pathologies. Severe organ disorder may even lead to death if undetected and treated in time (Prejbisz et al., 2011). In the present study, we found that around 30% of PPGL patients sought medical help because of paroxysmal symptoms (especially syncope (Wu HY et al., 2021)) induced by excessive catecholamines, while the rest were asymptomatic and were diagnosed through routine examination (Hamrin, 1962; Baxter et al., 1992; Ueda et al., 2005).

The preliminary screening of 293 samples identified 111 and 104 differential metabolites from the comparisons of PCC vs. healthy group and before vs. after surgery in the PCC group, respectively. A total of 65 differential metabolites presented a callback effect when comparing the healthy group and the post-surgical PCC group. By validation process of more samples, 53 differential metabolites in the comparison of PCC vs. healthy group were validated. In the comparison of before vs. after surgery, 53 differential

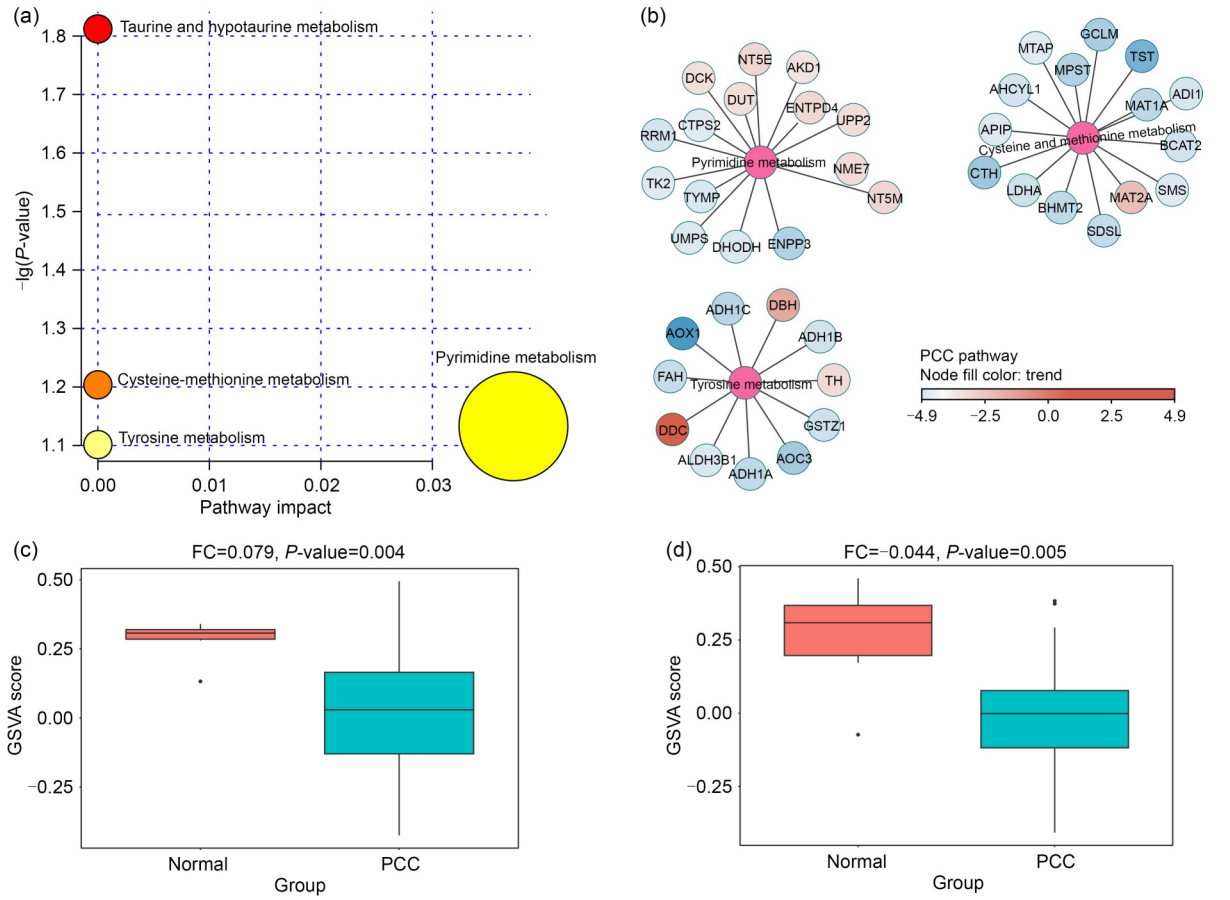

Fig. 4 Metabolic pathway analysis based on gene expression. (a) Pathway enrichment analysis by MetaboAnalyst. (b) Network of relationship between differential genes and pathways. (c) Tyrosine metabolism as a differential pathway based on gene set variation analysis (GSVA) score. (d) Cysteine-methionine metabolism as a differential pathway based on GSVA score. FC means fold change for mean score, with the *P*-value identified by Wilcoxon signed rank test. PCC: pheochromocytoma.

metabolites were also validated. A total of 37 differential metabolites in postoperative plasma had significant callback effects (Fig. 3, Tables S1–S6). Therefore, more than half of the differential metabolites were found to be altered because of the tumor removal surgery. Because of enhanced recovery after surgery, PPGL patients in our center are usually discharged within 48 or 72 h after surgery and the postsurgical plasma samples are taken before the patients are discharged. Therefore, the complete recovery of metabolic changes may not be fully witnessed. If we are able to obtain the follow-up plasma samples from the clinic, the recovery of more differential metabolites may be observed.

We matched the metabolic pathways of 53 differential metabolites obtained through validation, among which L-dihydroorotic acid, cyclic acid, and vanylglycol were successfully matched to the metabolic pathways. Based on the ROC curve, we found that L-dihydroorotic acid and vanylglycol have beneficial effects in the diagnosis of PCC. Furthermore, the combination model of the two substances may obtain better sensitivity and specificity in the prediction and diagnosis of PCC.

We next analyzed the DEGs between PCC and normal adrenal medulla using data from the GEO database. A total of 1814 genes were upregulated and 2016 genes were downregulated in PCC patients (Table S7). Through pathway matching, 42 genes were matched to the metabolic pathways. Synthesizing the metabolic pathways related to differential metabolites and those involved in DEGs, it was found that the cysteine-methionine metabolic pathway, tyrosine metabolic pathway, and pyrimidine metabolism pathway were the three main metabolic pathways affected in PCC patients. From the pathway enrichment analysis of DEGs, it was revealed that upregulated genes were

(a) LASSO model coefficients

Name	Dis (coefficient)	Val (coefficient)
Intercept	2.819 145	2.462 340
L-Dihydroorotic acid	0.425 340	0.605 894
Cysteic acid	0	0
Vanylglycol	−1.386 670	−1.320 780

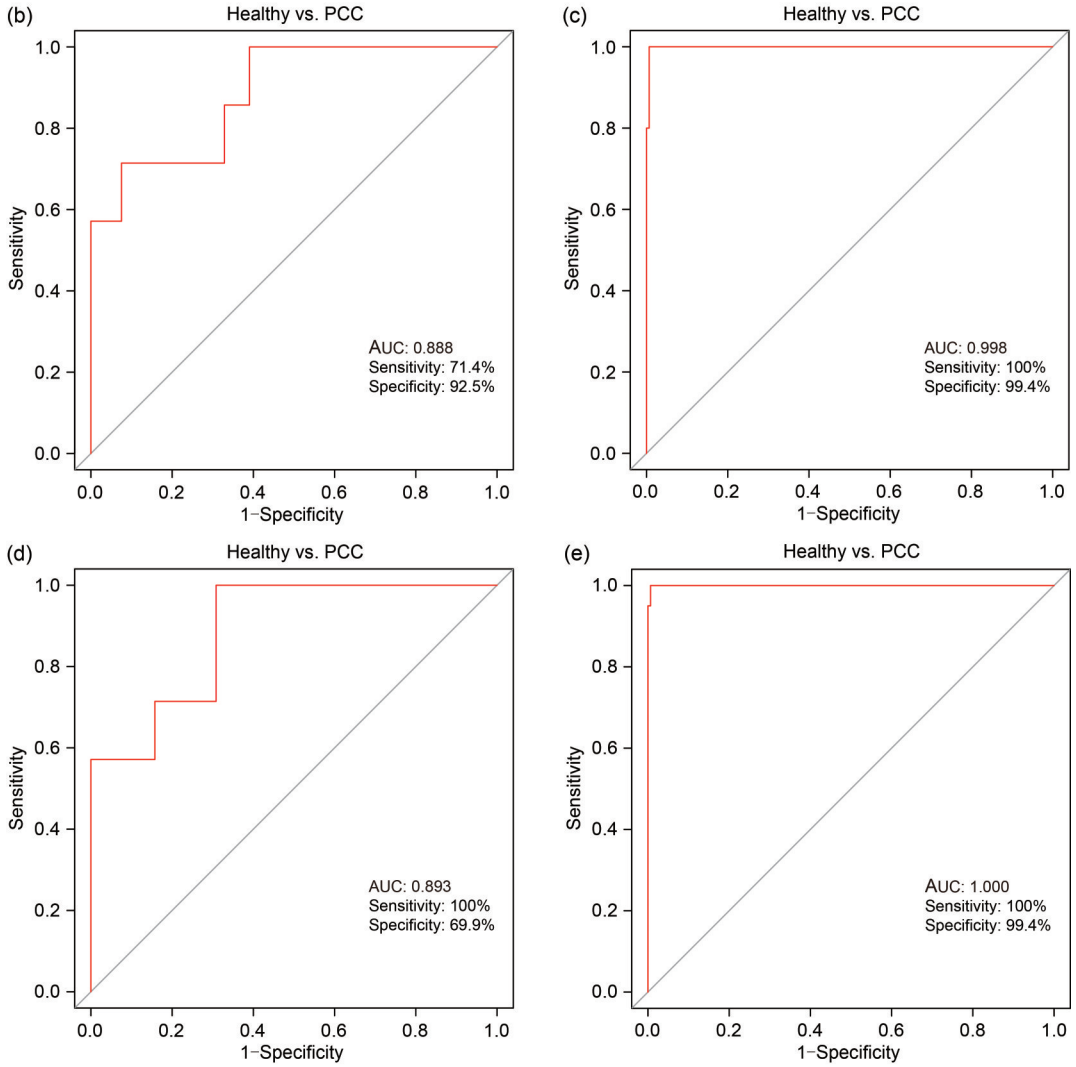

Fig. 5 Model for pheochromocytoma (PCC) diagnosis based on three metabolites. (a) The Least Absolute Shrinkage and Selection Operator (LASSO) model coefficients in the discovery (Dis) and validation (Val) sets. (b, c) The receiver operating characteristic (ROC) curves for L-dihydroorotic acid, cysteic acid, and vanylglycol. (d, e) The ROC curves for L-dihydroorotic acid and vanylglycol. (b, d) ROC curves for the Dis set. (c, e) ROC curves for the Val set. AUC: area under the curve.

mainly involved in the metabolic pathways related to neural activities involving axons, synapses, and neurotransmitters, which were associated with the origin of PCC from the neural crest. The downregulated genes were related to various metabolisms, including those of cholesterol, fatty acid, ethanol, sterol hormones, and nucleotides, and also conformed to the metabolic changes in PCC patients (Fig. S1).

Vanylglycol was a major differential metabolite found in this study, which is one of the end products of the catecholamine metabolic pathway. The result from MetaboAnalyst showed that the level of vanylglycol

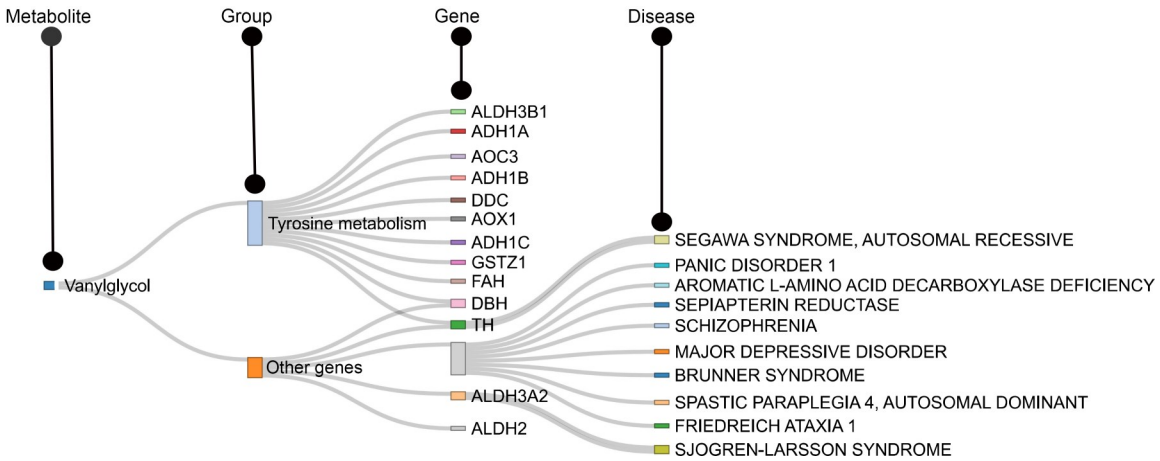

Fig. 6 Vanylglycol interaction network.

was related to mental disease (Fig. 6). Studies have shown that PCC patients were more likely to experience anxiety and depression, and the severity of symptoms positively correlated with the peripheral catecholamine levels (Starkman et al., 1990; Jia et al., 2021). Based on our results, vanylglycol may be another important biomarker for predicting psychological disorder. Moreover, early screening for anxiety and depression may be recommended for PPGL patients.

Based on the comprehensive analysis of metabolites and DEGs, we obtained the preliminary characteristics of metabolic changes in PCC patients. We found that the cysteine-methionine metabolic pathway, tyrosine metabolic pathway, and pyrimidine metabolic pathway were the main metabolic pathways affected by the neoplasm (Rehman et al., 2020; Zhou et al., 2021). These pathways were also closely associated with the clinical and pathological changes in PCC patients. Therefore, further research should look into the clinical intervention that may have effects on the above three pathways and maintain the normal metabolism of PCC patients in the perioperative period of PCC.

The unique strengths of our study include the exposure of metabolic changes in PCC patients and the exploration of targeted metabolic pathways. On the other hand, the limitations lie in the following three aspects: small sample size, incomplete biochemical indicators, and lack of long-term follow-up after surgery. To elucidate the molecular mechanism and metabolic changes of PCC, future exploration should focus on larger samples of clinical-pathological-molecular-metabolic matching data analysis to clarify the occurrence and development of PCC, so as to provide accurate solutions for early diagnosis and postoperative metabolic intervention.

5 Conclusions

In this study, we found that the cysteine-methionine metabolic pathway, tyrosine metabolic pathway, and pyrimidine metabolic pathway were three main metabolic pathways altered by the neoplasm in PCC. Based on the analysis of transcription levels, two pathways (tyrosine metabolism and cysteine-methionine) were downregulated in PCC and the pyrimidine pathway showed no significant difference. Meanwhile, we developed the optimized diagnostic model of two metabolites (L-dihydroorotic acid and vanylglycol). Our research suggests that L-dihydroorotic acid and vanylglycol metabolites could be potential clinical biomarkers to improve the diagnosis of PCC.

Data availability statement

All data generated or analyzed during this study can be made available by the corresponding author upon reasonable request.

Acknowledgments

This work was supported by the National Natural Science Foundation of China (No. 82072811).

Author contributions

Chong LAI, Qingrong SUN, and Maode LAI conceptualized and designed the study. Chong LAI and Renjie GONG collected samples and clinical data. Chong LAI, Qingling YANG, Yunuo ZHANG, Majie WANG, Jiankang LI, and Qingrong SUN performed the experiment and analyzed the data. Chong LAI,

Qingling YANG, Qingrong SUN, and Maode LAI wrote the initial draft. All authors have read and approved the final manuscript, and therefore, have full access to all the data in the study and take responsibility for the integrity and security of the data.

Compliance with ethics guidelines

Maode LAI is an Editorial Board Member for *Journal of Zhejiang University-SCIENCE B (Biomedicine & Biotechnology)* and was not involved in the editorial review or the decision to publish this article. Chong LAI, Qingling YANG, Yunuo ZHANG, Renjie GONG, Majie WANG, Jiankang LI, Maode LAI, and Qingrong SUN declare that they have no conflict of interest.

All procedures followed were in accordance with the ethical standards of the responsible committee on human experimentation (institutional and national) and with the Helsinki Declaration of 1975, as revised in 2013. Informed consent was obtained from all patients for being included in the study. The study protocol was approved by the Ethics Committee of the First Affiliated Hospital, Zhejiang University School of Medicine (No. IIT20230661A).

References

Aygun N, Uludag M, 2020. Pheochromocytoma and paraganglioma: from epidemiology to clinical findings. *Sisli Etfal Hastan Tip Bul*, 54(2):159-168. https://doi.org/10.14744/SEMB.2020.18794

Baxter MA, Hunter P, Thompson GR, et al., 1992. Phaeochromocytomas as a cause of hypotension. *Clin Endocrinol (Oxf)*, 37(3):304-306. https://doi.org/10.1111/j.1365-2265.1992.tb02326.x

Benjamini Y, Hochberg Y, 1995. Controlling the false discovery rate: a practical and powerful approach to multiple testing. *J R Stat Soc Series B Methodol*, 57(1):289-300. https://doi.org/10.1111/j.2517-6161.1995.tb02031.x

Chen PC, Wang CT, 2023. Rat pheochromocytoma PC12 cells in culture. *In*: Borges R (Ed.), Chromaffin Cells: Methods and Protocols. Humana, New York, p.3-15. https://doi.org/10.1007/978-1-0716-2671-9_1

Dwight T, Kim E, Novos T, et al., 2019. Metabolomics in the diagnosis of pheochromocytoma and paraganglioma. *Horm Metab Res*, 51(7):443-450. https://doi.org/10.1055/a-0926-3790

Eisenhofer G, Kopin IJ, Goldstein DS, 2004. Catecholamine metabolism: a contemporary view with implications for physiology and medicine. *Pharmacol Rev*, 56(3):331-349. https://doi.org/10.1124/pr.56.3.1

Erlic Z, Beuschlein F, 2019. Metabolic alterations in patients with pheochromocytoma. *Exp Clin Endocrinol Diabetes*, 127(2-3):129-136. https://doi.org/10.1055/a-0649-0960

Farrugia FA, Charalampopoulos A, 2019. Pheochromocytoma. *Endocr Regul*, 53(3):191-212. https://doi.org/10.2478/enr-2019-0020

Fluss R, Faraggi D, Reiser B, 2005. Estimation of the youden index and its associated cutoff point. *Biom J*, 47(4): 458-472. https://doi.org/10.1002/bimj.200410135

Hamrin B, 1962. Sustained hypotension and shock due to an adrenaline-secreting phaeochromocytoma. *Lancet*, 280(7247):123-124. https://doi.org/10.1016/s0140-6736(62)90006-5

Hänzelmann S, Castelo R, Guinney J, 2013. GSVA: gene set variation analysis for microarray and RNA-Seq data. *BMC Bioinformatics*, 14:7. https://doi.org/10.1186/1471-2105-14-7

Huang YY, Xu KL, Liu JY, et al., 2022. Promotion of adrenal pheochromocytoma (PC-12) cell proliferation and outgrowth using Schwann cell-laden gelatin methacrylate substrate. *Gels*, 8(2):84. https://doi.org/10.3390/gels8020084

Jia SM, Li CB, Lei ZQ, et al., 2021. Determinants of anxiety and depression among pheochromocytoma patients: a case-control study. *Medicine (Baltimore)*, 100(3):e24335. https://doi.org/10.1097/MD.0000000000024335

Jochmanova I, Pacak K, 2016. Pheochromocytoma: the first metabolic endocrine cancer. *Clin Cancer Res*, 22(20): 5001-5011. https://doi.org/10.1158/1078-0432.CCR-16-0606

Lee S, Nakamura E, Yang HF, et al., 2005. Neuronal apoptosis linked to EglN3 prolyl hydroxylase and familial pheochromocytoma genes: developmental culling and cancer. *Cancer Cell*, 8(2):155-167. https://doi.org/10.1016/j.ccr.2005.06.015

López-Jiménez E, Gómez-López G, Leandro-Garcia LJ, et al., 2010. Research resource: transcriptional profiling reveals different pseudohypoxic signatures in SDHB and VHL-related pheochromocytomas. *Mol Endocrinol*, 24(12): 2382-2391. https://doi.org/10.1210/me.2010-0256

Naranjo J, Dodd S, Martin YN, 2017. Perioperative management of pheochromocytoma. *J Cardiothorac Vasc Anesth*, 31(4):1427-1439. https://doi.org/10.1053/j.jvca.2017.02.023

Prejbisz A, Lenders JWM, Eisenhofer G, et al., 2011. Cardiovascular manifestations of phaeochromocytoma. *J Hypertens*, 29(11):2049-2060. https://doi.org/10.1097/HJH.0b013e32834a4ce9

Rehman T, Shabbir MA, Inam-Ur-Raheem M, et al., 2020. Cysteine and homocysteine as biomarker of various diseases. *Food Sci Nutr*, 8(9):4696-4707. https://doi.org/10.1002/fsn3.1818

Remacha L, Comino-Méndez I, Richter S, et al., 2017. Targeted exome sequencing of Krebs cycle genes reveals candidate cancer-predisposing mutations in pheochromocytomas and paragangliomas. *Clin Cancer Res*, 23(20):6315-6324. https://doi.org/10.1158/1078-0432.CCR-16-2250

Starkman MN, Cameron OG, Nesse RM, et al., 1990. Peripheral catecholamine levels and the symptoms of anxiety: studies in patients with and without pheochromocytoma. *Psychosom Med*, 52(2):129-142. https://doi.org/10.1097/00006842-199003000-00001

Ueda T, Oka N, Matsumoto A, et al., 2005. Pheochromocytoma presenting as recurrent hypotension and syncope.

Intern Med, 44(3):222-227.
https://doi.org/10.2169/internalmedicine.44.222

Wu HY, Gao TJ, Cao YW, et al., 2021. Case report: pheochromocytoma in a 59-year-old woman presenting with hypotension. *Front Cardiovasc Med*, 8:648725.
https://doi.org/10.3389/fcvm.2021.648725

Wu TZ, Hu EQ, Xu SB, et al., 2021. ClusterProfiler 4.0: a universal enrichment tool for interpreting omics data. *Innovation*, 2(3):100141.
https://doi.org/10.1016/j.xinn.2021.100141

Zhao HY, Zhao YZ, Jia YM, et al., 2021. Pheochromocytoma with abdominal aortic aneurysm presenting as recurrent dyspnea, hemoptysis, and hypotension: a case report. *World J Clin Cases*, 9(18):4754-4759.
https://doi.org/10.12998/wjcc.v9.i18.4754

Zhou Y, Tao L, Zhou X, et al., 2021. DHODH and cancer: promising prospects to be explored. *Cancer Metab*, 9(1):22.
https://doi.org/10.1186/s40170-021-00250-z

Zuber SM, Kantorovich V, Pacak K, 2011. Hypertension in pheochromocytoma: characteristics and treatment. *Endocrinol Metab Clin North Am*, 40(2):295-311.
https://doi.org/10.1016/j.ecl.2011.02.002

Supplementary information

Tables S1–S7; Figs. S1 and S2